Biochimica et Biophysica Acta, 1020 (1990) 49–56
Elsevier

BBABIO 43297

Structure of the ATP synthase from chloroplasts studied by electron microscopy. Localization of the small subunits

Egbert J. Boekema [1], Jianping Xiao [2] and Richard E. McCarty [2]

[1] *Biochemisch Laboratorium, Rijksuniversiteit Groningen, Groningen (The Netherlands) and* [2] *Section of Biochemistry, Molecular and Cell Biology, Division of Biological Sciences, Cornell University, Ithaca, NY (U.S.A)*

(Received 23 April 1990)

Key words: ATP synthase; Electron microscopy; Image analysis; Chloroplast

The structure of the hydrophilic part of the ATP synthase from chloroplasts (CF_1) has been further investigated by electron microscopy and image analysis of negatively stained samples. The projections of three different types of CF_1 were analyzed: the holoenzyme with five different subunits and two CF_1 particles depleted of δ and of δ,ϵ, respectively. About 1000 images of molecular projections of each of the three types were analyzed. They were aligned relative to different reference images and were then submitted to a multivariate statistical classification procedure. The analysis has been focussed on the projections of the hexagonal type. Comparisons between the average images of the three types of CF_1 and between the previously analyzed CF_1- and mitochondrial MF_1 ATP synthases clearly outline the many detailed similarities but also the differences. Removal of δ leads to a significant decrease in the diameter of CF_1: the distances between opposive large α and β subunits decrease by 1.3 nm. The additional removal of ϵ has no further effect on these distances. The positions of the small subunits could be localized within the $\alpha_3\beta_3$ structure. Subunit γ is located in the center of the hexagonal projection and has dimensions of 2.5–2.8 nm in the plane and about 5 nm in the vertical direction. Subunits δ and ϵ are located between γ and one pair of large α and β subunits, resulting in the V-shaped central mass, as found previously. The position of δ or ϵ is perhaps variable, since among the previously analyzed 3300 CF_1 projections, many projections were found with the central mass divided in two parts, with the smallest mass in different positions. Consequences of these findings for the mechanism of ATP synthesis are discussed.

Introduction

ATP synthesis/hydrolysis coupled with a transmembrane proton transport is carried out by a large membrane-bound enzyme (ATP-synthase) in different types of membrane (chloroplasts, mitochondria, bacteria). It consists of a membrane integrated part, F_0, which acts as a proton channel through the membrane and a hydrophilic part, F_1, which contains the nucleotide binding sites. The proton ATP-synthases from different sources have a very similar structure. This is especially the case for the F_1 part. F_1 ATP-synthase from spinach chloroplasts, CF_1, is composed of five different subunits: α (54 kDa), β (53.9 kDa), τ (35.7 kDa), δ (20 kDa) and ϵ (14.7 kDa). The molecular masses are estimated from the derived spinach amino acid sequences, as determined for β and ϵ [1], τ [2] and δ [3]. The gene coding for the α subunit has not been sequenced for spinach, but sequenced genes from other plant sources indicate a mass of about 54 kDa. One CF_1 molecule contains three copies of the large α and β subunits, and most likely one copy of the others. The ATP synthase structure and function have been reviewed extensively [4–8].

The structure of the soluble part of the ATP-synthase system has been studied by X-ray diffraction resulting in a low-resolution model [9], showing six regions of approximately equal size. The same regions can be visualized by electron microscopy, as well as a central seventh mass. In the so-called hexagonal view, the three α and β subunits are alternating [10–12]. From image reconstruction of (cryo-)electron micrographs a three-dimensional model was derived [13]. It shows that the large subunits are elongated. Since elongated masses have never been observed in negatively stained specimens [7,14], the three-dimensional shape of F_1 particles needs further attention.

Correspondence: E.J. Boekema, Biochemisch Laboratorium, Rijksuniversiteit Groningen, Nijenborgh 16, 9747 AG Groningen, The Netherlands.

In electron micrographs of negatively stained F_1, hexagonal projections ("top views") are very dominant. This is caused by preferential attachment of F_1 particles to the carbon support. Side views, which could give insight in the third direction of the molecule, are rare. Computer image analysis of single molecules in combination with multivariate statistical techniques were developed for analyzing mixed-populations of images [15]. The characteristic views, present in the population of images, are determined with an automatic classification scheme and the resulting class averages represent noise-reduced projection images of the molecule under investigation. In two earlier studies we applied these techniques to F_1 molecules from beef heart mitochondria (MF_1) [16] and spinach chloroplasts [17]. From these investigations it was concluded that in the hexagonal projection the central mass of subunits γ,δ and ϵ has the shape of the letter V. In CF_1, the central mass was often divided into two parts; the smaller one was interpreted as subunit δ. A further determination of the shape and localization of the small subunits was not possible from the holoenzymes. In the present study we have analyzed the hexagonal projections of CF_1, depleted of subunit δ and of subunits δ and ϵ. They have been compared with the projections from the holoenzyme CF_1.

Materials and Methods

CF_1 ATP-synthase was isolated from spinach chloroplasts as described in Ref. 18. $CF_1(-\delta)$ was prepared according to Patrie and McCarty [19]. $CF_1(-\delta,\epsilon)$ was prepared by ethanol treatment of $CF_1(-\delta)$ bound to DEAE-cellulose [20]. All samples were stored for several days as $(NH_4)_2SO_4$ precipitates at 0°C. The subunit composition of each preparation was tested by SDS-gel electrophoresis.

For electron microscopy, aliquots of the precipitated protein were dialyzed at room temperature (12 h) against 10 mM Tris-HCl (pH 8), containing 1 mM EDTA plus 2 mM ATP, and diluted afterwards 10–25x in the same buffer. Specimens were prepared using the droplet method with uranyl acetate as the negative stain. Electron microscopy was performed with a Philips EM 400 electron microscope. Micrographs used for the analysis were taken with 80 kV at 60,000 magnification. Care was taken not to preilluminate the part of the specimen to be recorded, to avoid excessive specimen damage. To allow comparison between the three types of CF_1 particle, the samples and the electron microscopy procedures were standarized as much as possible; for instance, carbon support films were from the same batch.

Selected micrographs were digitized with a Joyce-Loebl Scandig 3 rotating drum densitometer using a step size of 25 μm, corresponding to a pixel (image element) size of approx. 0.4 nm at the specimen level. Image analysis was carried out on a Convex C1-XP mini-supercomputer using IMAGIC software [21].

Particles were selected interactively from the micrographs using a raster-scan image display system. A total of about 3000 molecular images was extracted from 15 different micrographs, using a window of 48×48 pixels. They were pretreated by band-pass filtering to suppress the very low and very high spatial frequencies which normally do not contain useful information and may influence the alignment procedures [16,17]. Unnecessary background of the images was masked out by a circular mask with a radius of 21 pixels. The average density inside the mask was set to zero and the variance of densities was normalized to an arbitrary value of 100. The next steps in the analysis, the alignment of the images, the eigenvector-eigenvalue data compression procedure ("correspondence analysis") and the classification were carried out essentially as described previously [16,17].

Results

Analysis of hexagonal projections

By the negative staining technique, a sufficient number of good quality electron micrographs of three types of CF_1, differing in the number of small subunits was obtained. Fig. 1 shows a field of $CF_1(-\delta)$ particles, as an example for an electron micrograph used for image analysis. Most particles were well preserved. From 15 of

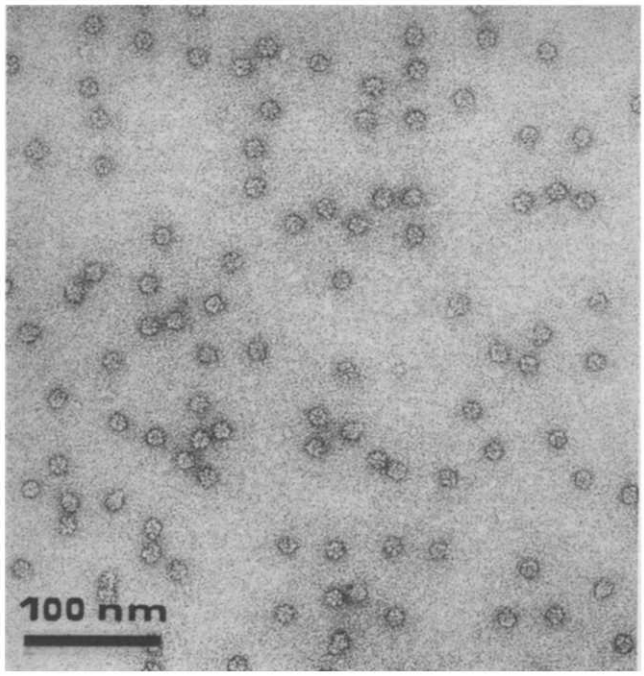

Fig. 1. Part of an original electron micrograph showing molecules of F_1 ATP-synthase used for the analysis of single particles. These particles lack subunit δ and were negatively stained with a 1% solution of uranyl acetate.

such negatives about 3000 molecular projections were extracted for image processing, 1000 for each of the three types of CF_1. Almost all projections were of a hexagonal shape. The image analysis was carried out separately for each of the three data sets, but the same scheme of the subsequent steps was followed in the alignment of the projections, the multivarite statistical analysis and the classification. We started with a six-fold symmetrized reference, in order to centre the projections. All further 10 alignments cycles were carried out with improved references made from the previous alignment. Then it was followed by a first multivariate statistical analysis (MSA) plus classification (not shown) in which the three data sets were decomposed into eight classes, automatically rejecting about 15% of the projections. The rejected images mainly seem to represent badly aligned particles, and particles which were stained in a non-typical way. By examining the sums of the class members, the central mass, which is more or less V-shaped and bound to one α,β-pair [16], was found mostly in the same position. In some classes, however, it was rotated over 60°. As next references we therefore took the sums of the best classes with the central mass in the same position. The three data sets were re-aligned with this final reference and the analysis was repeated. Finally the data sets were decomposed into six classes for each of the three CF_1 preparations. These results are shown in Figs. 2–4.

Figs. 2–4 show the variation as present in the data sets. Most classes are quite similar, although some may represent more strongly distorted projections, such as the class of Fig. 3A. In all three cases, however, the final six classes appear quite similar which means that the projections must all have been brought into the same position by the alignments and classification. The remaining differences between the classes seem to represent largely noise. Three final sums of particles were therefore made straightforwardly from the best classes (Fig. 6). They represent the better 70% of the projections. Besides the rejection of 15% of the projections during the multivariate statistical analysis (MSA) and the omission of some of the final classes, 5–10% of the projections was rejected already before the MSA step on the base of a very low correlation coefficient between projection and reference. Visual examination of all these projections showed that the latter ones largely were misaligned.

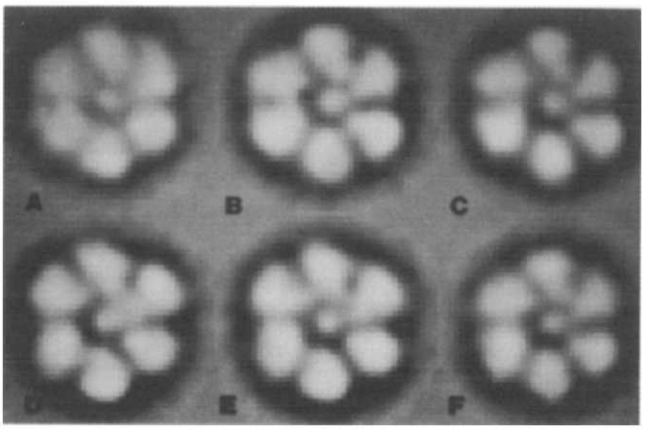

Fig. 3. Image analysis of the 4-subunit $CF_1(-\delta)$ particles. The molecular projections of this CF_1 ATP-synthase were determined with the same procedure as for those of $CF_1(-\delta,\epsilon)$ in fig. 2, but the analysis was carried out independently. In the final classification step the data set of 986 molecules was decomposed into six classes (A–F) with numbers of class members: A, 148; B, 144; C, 151; D, 132; E, 152 and F, 112.

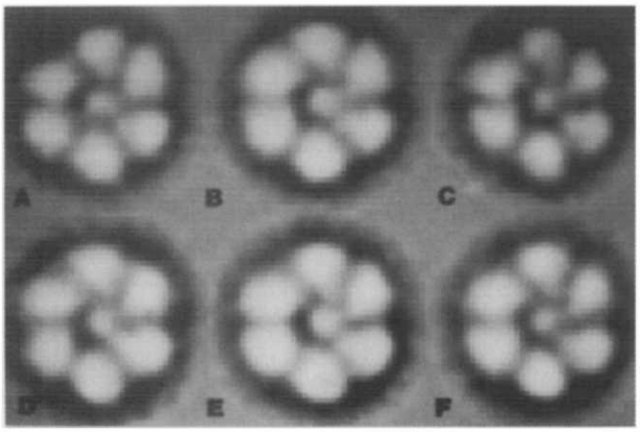

Fig. 2. Image analysis of the 3-subunit $CF_1(-\delta,\epsilon)$ particles. Molecular projections of CF_1 ATP-synthase as determined by multireference alignments and classification of 802 molecules; the final six classes (A–F) show the image variation present in the data set. Number of class members: A, 128; B, 127; C, 75; D, 68; E, 170 and F, 155, respectively. Note: the images are shown with imposed band-pass filter, which is necessary for the suppression of unwanted noise during analysis. This filter allows a better analysis of the image features, but has the disadvantage to suppress the central density (see also Fig. 6).

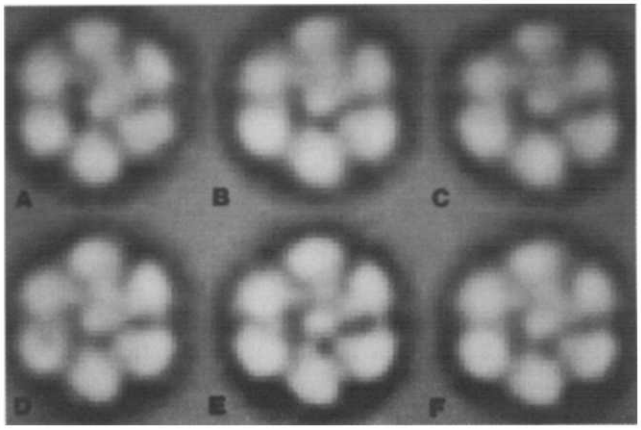

Fig. 4. Image analysis of the 5-subunit CF_1 particles. The molecular projections the holoenzyme CF_1 ATP-synthase were determined as explained for Figs. 2 and 3. In the final classification step the data set of 1019 projections was decomposed into six classes (A–F) with numbers of class members of: A, 93; B, 155; C, 120; D, 174; E, 101 and F, 158.

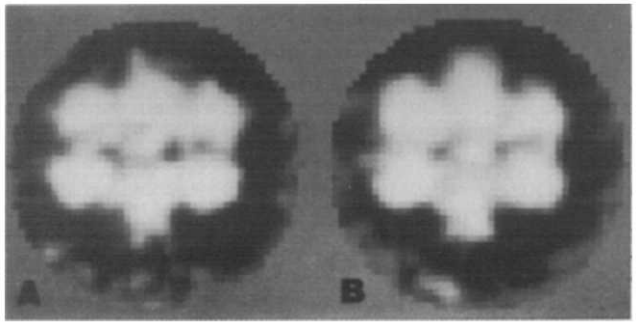

Fig. 5. Analysis of the rare side views of holoenzyme CF_1. The 70 projections were aligned and two sets of 13 (A) and 23 (B) similar appearing projections were summed.

Analysis of side views

To obtain insight into the three-dimensional structure of CF_1 it is important to analyze side views of molecules as well. An examination of the holoenzyme data set of about 1000 particles showed that 70 were of a side-view type, clearly different from the hexagonal views. They were selected and analyzed. After repeated alignments on improved references two sets of the best 13 and 23 aligned projections were averaged (Fig. 5). Although the features are not very defined due to the low signal-to-noise ratio, both sums show a projected structure in the form of a flattened hexagon. Seven protein densities can be recognized.

Discussion

Many pitfalls are possible during the images analysis, which includes dozens of small subsequent steps. Small details as seen in averaged projections may therefore be artefacts rather than real features of the studied objects. Moreover, the negative stain, which is necessary for the image contrast can also be the cause of rearrangements in projections. Nevertheless, the similarities between the average hexagonal projections of the CF_1 and MF_1 holoenzymes (Figs. 6C and 7J), which were analyzed independently, is very striking. The V-shaped central mass has the same shape, as well as the cleft and the groove between neighboring large subunits (for an explanation of these terms, see Figs. 7,8). In both cases, the "leg" of the the V-shaped mass beside the cleft is slightly more substantial than the other one. The simi-

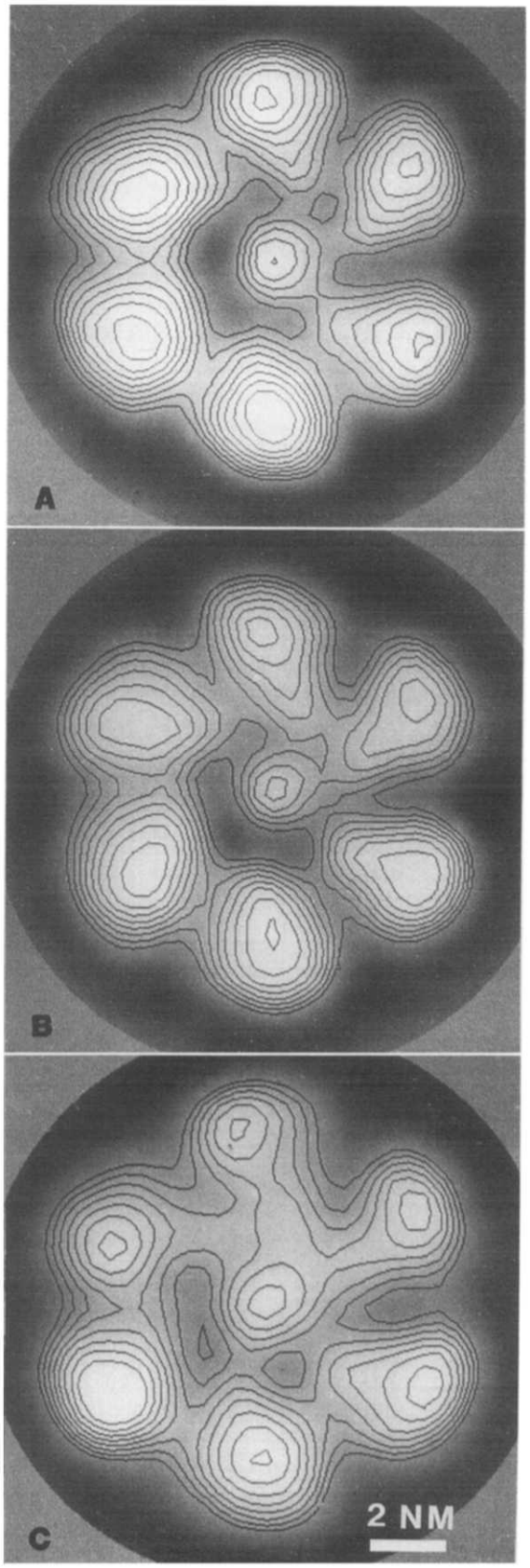

Fig. 6. Comparison of the average projections of three types of CF_1 particle (A) the $CF_1(-\delta,\epsilon)$ particle, a sum of 580 projections from 4 classes of Fig. 2A,B,E,F; (B) the $CF_1(-\delta)$ particle, a sum of 691 projections from five classes of Fig. 3B-F; (C) the holoenzyme CF_1 particle, a sum of 802 projections from six classes of Fig. 4A–F. The three final sums are from projections with the original image components, i.e. without the band-pass filter imposed during alignment, MSA and classification. The sums have been contoured with equidistant density levels, in order to facilitate the features of the original stain distribution.

larities between both average projections let us conclude that the features seen in the projections must be related to the F_1 ATP synthase structure. This facilitates an interpretation of the projections of the holoenzyme F_1 and also of the projections of $CF_1(-\delta)$ and $CF_1(-\delta,\epsilon)$, where a similar cleft between two large subunits is visible in the right part of the projection.

Interpretation of the average projections

Fig. 6A shows the average hexagonal projection of $CF_1(-\delta,\epsilon)$. The six peripheral masses form the $\alpha_3\beta_3$ hexagon. The seventh mass, the γ subunit, is located almost exactly in the center, although it seems to have more interaction with the large subunits in the upper right half of the image. The projected γ subunit measures only about 2.5–2.8 nm in diameter. Since it has to fit a mass of 35.7 kDa [2], this means that γ is an elongated subunit with a calculated length of about 5 nm, supposing a protein density of 1.3.

The shape and diameter of the average projections of $CF_1(-\delta,\epsilon)$ and $CF_1(-\delta)$ are very similar (Figs. 6A,B). Between the central mass and the upper right masses of Fig. 6B there is, however, more density present. This density is interpreted as being the ϵ subunit. Its location is indicated in Fig. 8. Fig. 6C shows the average view of holoenzyme CF_1. Its diameter is larger in comparison to the other two projections. This means that removal of δ leads to a significant decrease in the diameter of CF_1; the distances between the centers of opposive large α and β subunits decrease by 1.3 nm. In other words: subunit δ alters the positions of the α and β subunits relative to each other. This is in line with results of Schinkel and Hammes [22], who have found that removal of the δ subunit resulted in a 25% smaller rotational correlation time, although the δ subunit contributes only 5% of the mass of CF_1.

Subunit δ has a very elongated shape and is largely buried within the CF_1 structure [23,24]. Its location within the CF_1 hexagonal projection is also possible, from the differences between Fig. 6C and Figs. 6A and 6B. A comparison shows that the left part ("leg") of the V-shaped mass connecting the central mass to two outer subunits is clearly more substantial in Fig. 6C. This is accompanied by the appearance of a new "bridge" between this mass and a large subunit on the left. The same features were previuosly found for MF_1 (Fig. 7J) where the right part of the V-shaped mass, beside the cleft, was also less substantial than the left part. The "bridge" feature was also visible, although less pronounced. Examination of the original classes of Fig. 5 in Ref. 16, shows that most have a clear bridge, except for the class of Fig. 5E. In that case the disappearance of the bridge was accompanied by the appearance of additional mass close to large subunits opposive to the large subunits connected with the V-shaped mass. From all these observations it is deduced that the δ subunit

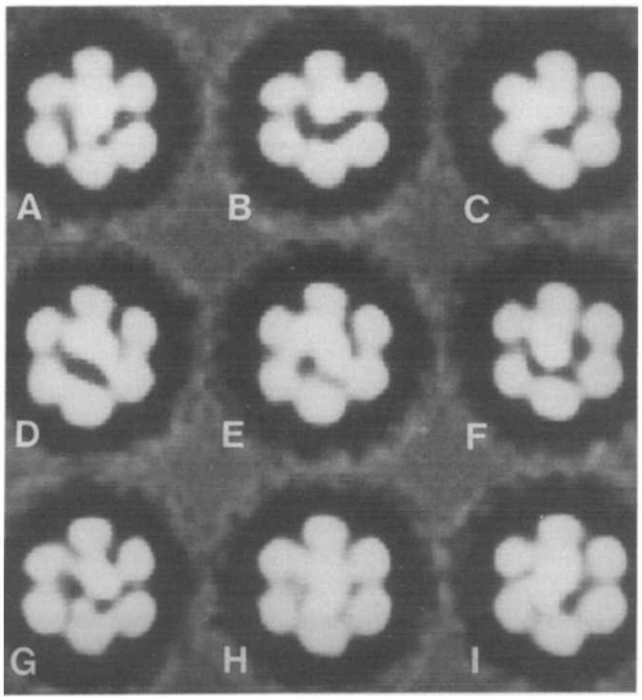

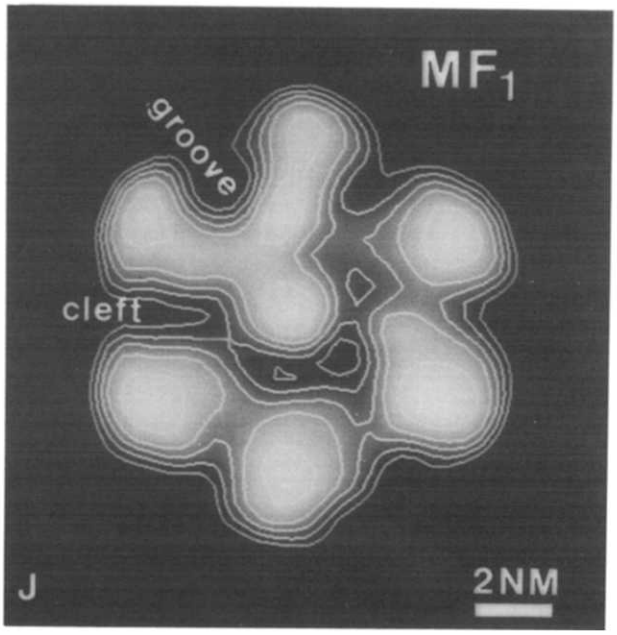

Fig. 7. Comparison of the results of image analysis of average projections of holoenzyme F_1 ATP synthases. (A–I) Nine original classes of CF_1 projections, taken from Fig. 3 of ref. [17]; (J) Final image of 379 projections of mitochondrial $(M)F_1$, from Ref. 16. Remark: The CF_1 and MF_1 holoenzyme projections are both asymmetric. This means that they show a handedness. During the processing of the micrographs of [16,17] a mirror inversion was automatically introduced by the digitizing camera. To facilitate the comparison with the new data, the original CF1 classes are now shown in their mirrored version. The preferential attachment of F_1 particles to the carbon support film mainly leads to hexagonal projections with the "cleft" (see Fig. 8) on the right side beneath the V-shaped mass. The sum of (J) is exactly as presented in Ref. 16 and its mirror-version is similar to Fig. 6C.

must be localized beneath the thickest leg of the V-shaped mass and the bridge. Comparison with the previous analysis of 3300 CF_1 projections [17], reproduced in Figs. 7A–I, is also of interest and further supports this deduction. Although some classes, such as Fig. 7B, have the same features (V-shaped mass, cleft and bridge) at the same place, other classes are different and apparently that data set was more inhomogeneous in regard of the positions of the central subunits. In most classes, the V-shaped mass was also connected to other (opposive) large subunits (Figs. 7D,E) or even split into a smaller and larger part (Fig. 7G). We assume that subunit γ remains centrally located in the average holoenzyme CF_1 projection of Fig. 6C, since Mitra and Hammes [25] have found that there is no structural change in the γ subunit after removal of δ and ϵ subunits and because γ has a strong interaction with the α and β subunits [26,27]. The large differences of the various classes of [17] are then merely caused by different positions of δ in relation to the other subunits. When subunit γ always remains in the central position within the $\alpha_3\beta_3$ hexagon, the open space around τ is quite symmetrically shaped and δ could fit in several positions within the $\alpha_3\beta_3$ structure. In principle, it seems possible that even a second δ subunit could be fitted within the hexagon without too much structural constraint. This idea is not unrealistic, because in mitochondrial MF_1 ATP synthase, the OSCP subunit, which has structural similarities to chloroplast δ, is present in the stalk, although it was absent from the particles analyzed in Ref. 16. Furthermore, it is noteworthy in this context that on F_1 binding sites with different affinities were found for δ [23].

Our findings are based on the interpretation of the hexagonal projections or top views of CF_1, since other projections (Fig. 5) are less frequent and more difficult to interprete at high resolution. All 3000 projections, used for the analysis, were visually inspected several times before, in order to exclude most of the side views and the so-called "flattened-hexagonal projections" [17], where the staining is sometimes quite uneven. The final result of the analysis (Fig. 6C), however, still shows a slight uneven stain distribution around the projection (not shown). As a result, the large subunits on the side of the V-shaped central mass are always in a thicker layer of stain, making them slightly smaller in projection (Fig. 6C). This phenomenon has been extensively discussed before [17]. Interestingly, in the filtered projection of crystals of a thermophilic ATPase [28] the asymmetric mass is also on the side of the smaller-appearing large subunits. By filtering away the stain gradient from Fig. 6C, the large subunits on the side of the V-shaped central mass slightly regain their full diameter (Fig. 8). Since the preferential staining is less pronounced in Figs. 6A-B, we think that the δ subunit must be directly or indirectly responsible for preferential staining. The most simple explanation for this would be that δ is slightly extending the F_1 structure, causing some tilt of the hexagon out of the plane. Slight tilting could result in a slight overlap of the central mass and the smaller looking outer subunits in projection. Slight tilting is, however, difficult to (dis)prove [17], since differences in the projected positions of the large subunits will always be marginal. Moreover, the stain distribution is somewhat inhomogeneous. This tends to deform slightly the shape of the projection. We are therefore unable to give a satisfying answer to the question why the groove in the upper part of the projection, indicated in Fig. 8, widens from Fig. 6A to 6B to 6C. It could be tilting of the total F_1 structure, but a change in the position of only two α,β large subunits relative to the other ones is also possible. Nevertheless, out of the three projections of Fig. 6 the one of Fig. 6C is significantly larger than the others. The difference cannot be caused by merely tilting, because the hexagonal view is always the largest projection of all and eventual tilting only leads to smaller-appearing projections.

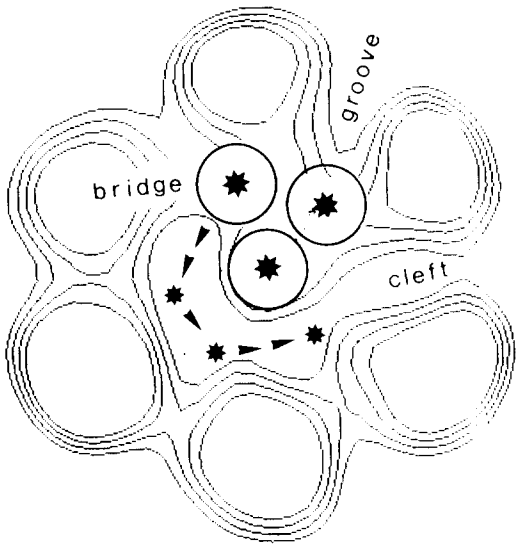

Fig. 8. An outline of the top view projection of CF_1 ATP synthase, with characteristic features ("cleft", "groove" and "bridge") indicated. The positions of the small subunits within the $\alpha_3\beta_3$ subunit ring have been indicated by asterisks; the central lower one being γ, the upper right one ϵ and the upper left one δ. Possible alternative positions of δ or ϵ, as found by classification of projections, are indicated by smaller asterisks.

Three-dimensional structure

Recently, Gogol and co-workers have presented a model for the three-dimensional structure of F_1 ATP synthase, based on tilted images of crystals and on average views of single particles [13]. Although this work has been well performed, the conclusion (the elongated form of the α and β subunits) is likely an overinterpretation of their data. Moreover, the interpre-

tation of the side views is inconsistent. According to Fig. 8 of Ref. 13, projections of the structure from the side should mainly belong to two different types, called bilobed and trilobed views. This idea is essentially correct. This is concluded from a similar case of an object with mainly one hexagonal top view and two different types of side view [29]. However, if the model with elongated subunits is correct, there is no explanation why the bilobed view is substantially longer than the trilobed view (Fig. 7). Furthermore, the protrusion on the right side of the bilobed view is unexpected. Also, the shape of the two outer masses on the trilobed view is inconsistent with the model, because they have an intrusion in the center. These observations weaken the conclusions of the model. The only remaining evidence for elongated subunits comes from the three-dimensional reconstruction [13]. The crucial quality parameter of a reconstruction is the resolution in the direction vertical to the plane of the untilted crystal. Limited maximal tilting leads to a resolution that is lower than the resolution in the untilted plane [30]. The authors claim a resolution of 2.4 nm in the plane and 3 nm in the reconstruction. However, the (1,3) diffraction spots of the crystals indicate a resolution of about 3.7 nm, instead of 2.4 nm. Therefore the resolution in the reconstruction is only about 4–5 nm and the exact shape of the large subunits seems to be difficult to verify. We can therefore only conclude that the exact shape of the large subunits is unknown. The shape may be (slightly) elongated or about spherical, as has been previously found or suggested [9,31,14,7].

We think that an arrangement into two layers of three about spherical subunits is still the most likely model for F_1, since such an arrangement can fully explain the various projections. If, for instance, the bilobed view (Fig. 7A of Ref. 13) is rotated over 90°, the interpretation is consistent. The width would then be similar to the maximal diameter of the hexagonal view, the distance between one α and one β (Fig. 6 in Ref. 13). The width of trilobed view of Ref. 13 is similar to the maximal distance between two α or two β subunits in the hexagonal projection. But if the bilobed view is rotated over 90°, there is no longer evidence for elongated large subunits, since the large cleft is now running horizontally through the projection. In fact, this cleft is slightly visible in the trilobed view as well. The small number of side-view projections, analyzed from the holoenzyme CF_1 (Fig. 5) shows that in the negative stained samples two groups of side views exist which resemble those seen in the frozen-hydrated samples of [13]. We have previously found very similar projections for MF_1 (Fig. 5H of Ref. 16) and CF_1 (unpublished data). The main difference between Fig. 5A and the bilobed view of Ref. 13 is that the individual large subunits are visible in 5A. Figs. 5A and B show the $\alpha_3\beta_3$ structure in a tilted position, in comparison to the hexagonal view. The large subunits still look about spherical. This is evidence for a two-layered model of rather spherical large subunits and clearly not for a model with elongated subunits. However, for further details on the three-dimensional structure, analysis of at least a thousand side views is necessary. With negatively stained specimens this has not been possible; the preferential attachment of F_1 particles to the carbon support almost exclusively results in hexagonal projections and the number of side views is rare.

Closing remarks

Our localization of the small subunits can be compared with the results from others. Hammes and coworkers have determined several distances within the CF_1 structure from fluorescence resonance energy transfer measurements [32,33]. A distance of 4.2–4.5 nm was measured between a sulfhydryl-group and the S–S disulfide bridge within subunit γ. In their model, this distance was placed under an angle of about 45° relative to the membrane. Our overall dimensions of γ ($2.5–3 \times 5–6$ nm) indicate that these sites must indeed be on different height from the membrane and from this it can be further concluded that the hexagonal view is parallel to the membrane [7]. Our results confirm that a part of subunit γ is in the center of the structure and furthermore, the asymmetric localization of the ϵ subunit. The S–S disulfide bridge [33] is possibly located on a protrusion of the γ structure, since the density of subunit γ is largely restricted to the center of the hexagonal projection. Perhaps it is localized in the connecting density between subunit γ and the large subunits in the upper right of Fig. 6A. Our results also confirm electron microscopic studies on MF_1 using a ferritin label [34], in which was found that γ and/or ϵ are asymmetrically oriented.

Gogol et al. have found that trypsin digestion of *E. coli* F_1 ATP synthase causes the loss of subunits δ and ϵ, as well as a cleft in subunit γ. Together, this reduces the diameter of the F_1 projection [12]. We now have shown more directly that the removal of the δ subunit leads to a smaller diameter and therefore to a rearrangement of the large subunits. This phenomenon could also have a more genereal significance. In theory it is possible that a change in the position of δ leads to conformational changes in the CF_1 structure generated during energy conversion at the catalytic sites. Since δ is also part of the stalk connecting F_1 to the membrane-bound F_0 [35], the other item, the energy-link from the proton gradient over the membrane to F_1, comes to mind as well. At the low resolution of electron microscopy, it is only possible to visualize large changes in the conformation of CF_1. Eventual movements in the vertical direction, along the stalk, cannot be detected from the top views. But changes in the position of the δ subunit,

caused by a rotational shift in the plane of the F_1 subunit, as schematically drawn in Fig. 8, can be registrated by electron microscopy and image analysis. Especially the results shown in Fig. 7A–I suggest that subunit δ or ϵ can be in structurally different positions. At the moment an explanation of this phenomenon is still open. Possibly, artifactal deformations of the F_1 structure could already give rise to the observed differences of the position of δ or ϵ in the various projections. But in the light of the function of ATP synthase real conformational changes, the alternative explanation, cannot be ruled out. A logical next step will therefore be to study projections from CF_1 particles in different forms (catalytically active/inactive). Such investigations could be helpful in narrowing down the number of possibilities how the mechanism of ATP synthesis at the atomic level really takes place.

Acknowledgements

We wish to thank Professor E.F.J. van Bruggen for general support, Dr. W. Keegstra for his help with computer image analysis, Mr. K. Gilissen and Mr. J. Haker for technical assistance and Professor P. Gräber for discussions. The research of E.J.B. has been made possible by a fellowship of the Royal Netherlands Academy of Arts and Sciences.

References

1 Zurawski, G., Bottomley, W. and Whitfeld, P.R. (1982) Proc. Natl. Acad. Sci. USA 79, 6260–6264.
2 Hermans, J., Rother, Ch., Bichler, J., Stepphuhn, J. and Herrmann, R.G. (1988) Plant Mol. Biol. 10, 323–330.
3 Miki, J., Maeda, M., Mukohata, Y. and Futai, M. (1988) FEBS Lett. 232, 221–226.
4 Strotmann, H. and Bickel-Sandkötter, S. (1984) Annu. Rev. Plant Physiol. 35, 97–120.
5 Senior, A.E. (1988) Physiol. Rev. 68, 177–231.
6 McCarty, R.E. and Nalin, C.M. (1986) in Photosynthesis III (Staehelin, L.A. and Arntzen C.J., eds.), Springer, Berlin.
7 Brink, J., Boekema, E.J. and Van Bruggen, E.F.J. (1988) Electron Microsc. Rev. 1, 175–199.
8 Tiedge, H. and Schäfer, G. (1989) Biochim. Biophys. Acta 977, 1–9.
9 Amzel, L.M., McKinnney, M., Narayanan, P. and Pedersen, P.L. (1982) Proc. Natl. Acad. Sci. USA 79, 5852–5856.
10 Tiedge, H., Lünsdorf, H., Schäfer, G. and Schairer, H.U. (1985) Proc. Natl. Acad. Sci. USA 82, 7874–7878.
11 Lünsdorf, H., Ehrig, K., Friedl, P. and Schairer, H.U. (1985) J. Mol. Biol. 173, 131–136.
12 Gogol, E.P., Aggeler, R., Sagermann, M. and Capaldi, R.A. (1989) Biochemistry 28, 4717–4724.
13 Gogol, E.P., Lücken, U., Bork, T. and Capaldi, R.A. (1989) Biochemistry 28, 4709–4716.
14 Tsuprun, V.L., Mesyanzhinova, I.V., Kozlov, I.A. and Orlova, E.V. (1984) FEBS Lett. 167, 285–290.
15 Van Heel, M. and Frank, J. (1981) Ultramicroscopy 6, 187–194.
16 Boekema, E.J., Berden, J.A. and Van Heel, M.G. (1986) Biochim. Biophys. Acta 851, 353–360.
17 Boekema, E.J., Van Heel, M. and Gräber, P. (1988) Biochim. Biophys. Acta 933, 365–371.
18 Shapiro, A.B. and McCarty, R.E. (1990) J. Biol. Chem. 265, 4340–4347.
19 Patrie, W.J. and McCarty, R.E. (1984) J. Biol. Chem. 259, 11121–11128.
20 Richter, M.L., Patrie, W.J. and McCarty, R.E. (1984) J. Biol. Chem. 259, 7371–7373.
21 Van Heel, M.G. and Keegstra, W. (1981) Ultramicroscopy 7, 113–130.
22 Schinkel, J.E. and Hammes, G.G. (1986) Biochemistry 25, 4066–4071.
23 Wagner, R., Apley, E.C., Engelbrecht, S. and Junge, W. (1988) FEBS Lett. 230, 109–115.
24 Finke, W. and Berzborn, R.J. (1990) in Current Research in Photosynthesis (Baltscheffsky, M., ed.), Vol. 3, 57–60, Kluwer, Dordrecht.
25 Mitra, B. and Hammes, G.G. (1988) Biochemistry 27, 245–250.
26 Moroney, J. and McCarty, R.E. (1982) J. Biol. Chem. 257, 5910–5914.
27 Smith, J.B. and Sternweis, P.C. (1983) Arch. Biochem. Biophys. 217, 376–378.
28 Yoshimura, H., Endo, S., Matsumoto, M., Nagayama, K. and Kagawa, Y. (1989) J. Biochem. 106, 958–960.
29 Boekema, E.J. and Van Heel, M. (1989) Biochim. Biophys. Acta 957, 370–379.
30 Crowther, R.A., De Rosier, D.J. and Klug, A. (1970) Proc. R. Soc. (London) A317, 319–340.
31 Tiedge, H., Schäfer, G. and Mayer, F. (1983) Eur. J. Biochem. 132, 37–45.
32 Snyder, B. and Hammes, G.G. (1984) Biochemistry 23 5787–5795.
33 McCarty, R.E. and Hammes, G.G. (1987) Trends Biochem. Sci. 12, 234–237.
34 Tsuprun, V.L., Mesyanzhinova, I.V., Milgrom, Y.M. and Kalashnikova, T.Y. (1987) Biochim. Biophys. Acta 892, 130–137
35 Engelbrecht, S. and Junge, W. (1990) Biochim. Biophys. Acta 1015, 379–390.